IL NUOVO CIMENTO VOL. VI, N. 4 1° Ottobre 1957

Inelastic Scattering of 150 MeV Negative Pions by Carbon and Lead (*+).

R. H. MILLER

The Enrico Fermi Institute for Nuclear Studies
The University of Chicago - Chicago, Ill.

(ricevuto il 1° Luglio 1957)

Summary. — Energy sensitive counters of the Čerenkov or scintillation type were used in conjunction with a pulse height analyzer to measure the energy spectrum of 150 MeV negative pions scattered from carbon or lead at various angles. Most of the pions scattered into the backward hemisphere had an energy less than 40 MeV. This is in contrast to the result of a Monte Carlo calculation based on a simple Fermi gas model, in which most of the pions scattered backwards have energies above 60 MeV. The measurements indicate that the absorption of pions by carbon is about that predicted by the Monte Carlo calculation, while the absorption by lead is about $\frac{1}{4}$ that expected.

1. – Introduction.

Although the scattering of pions with protons has been studied rather extensively (1), the experimental information on the scattering with complex

(*) Research supported by a joint program of the Office of Naval Research and the U.S. Atomic Energy Commission.

(+) Based on a thesis submitted to the Faculty of the Department of Physics, the University of Chicago, in partial fulfilment of the requirements for the Ph.D. degree.

(1) H. L. ANDERSON: *Proceedings of the Sixth Annual Rochester Conference* (New York, 1956), p. I-20.

nuclei is still very meagre ([2-4]). Considerable interest attaches to the extent to which simple models are capable of giving a good description of the processes involved ([5,6]). In these models the scattering is constructed from the pion-nucleon interactions, which are assumed not to be appreciably modified within nuclei, while the absorption is supposed due to the process $\pi^- + D = N + N$ ([7]). The knowledge of these fundamental processes is now sufficient so that definite predictions may be obtained from the models. The present series of experiments was undertaken to improve in accuracy and detail the knowledge of the interaction of pions with complex nuclei. This paper deals with the energy and angular distribution of 150 MeV negative pions observed to be inelastically scattered from carbon or lead. Negative pions were used because of the greater flux available. The energy was chosen as near the 180 MeV pion-nucleon scattering resonance as was consistent with high counting rates. This has the effect of maximizing the inelastic processes since the cross-section for the individual pion-nucleon scattering is a maximum here while the real part of its amplitude in the forward direction is small. Thus there should be little elastic contribution to the total scattering other than diffraction and Coulomb scattering. The results are compared with Monte Carlo calculations kindly carried out for this purpose by METROPOLIS *et al.* ([8]) on a simple Fermi gas model. A paper by T. FUJII ([9]) will describe the observations of the elastic scattering and make the comparison with a simple optical model using potentials calculated by WATSON *et al.* ([5]) from the knowledge of the fundamental scattering and absorption processes. It will be shown that while these models have a certain utility in giving the general characteristics of the interaction, they fail to give correctly most of the detailed behavior observed in these experiments.

([2]) A. E. IGNATENKO: *Proceedings of the CERN Symposium* (CERN Organization for Nuclear Research, Geneva, 1956), Vol. **2**, p. 313. A review of Russian work.

([3]) H. BYFIELD, J. KESSLER and L. LEDERMAN: *Phys. Rev.*, **86**, 17 (1952); J. KESSLER and L. LEDERMAN: *Phys. Rev.*, **94**, 689 (1954).

([4]) P. ISAACS, A. SACHS and J. STEINBERGER: *Phys. Rev.*, **85**, 718 (1952); A. PEVSNER, J. RAINWATER, R. E. WILLIAMS and S. J. LINDENBAUM: *Phys. Rev.*, **100**, 1419 (1955); R. E. WILLIAMS, J. RAINWATER and A. PEVSNER: *Phys. Rev.*, **101**, 412 (1956); R. E. WILLIAMS, W. F. BAKER and J. RAINWATER: *Phys. Rev.*, **104**, 1695 (1956); W. F. BAKER, J. RAINWATER and E. R. WILLIAMS: *Bull. Am. Phys. Soc.*, **2**, 6 (1957).

([5]) R. M. FRANK, J. L. GAMMEL and K. M. WATSON: *Phys. Rev.*, **101**, 891 (1956).

([6]) M. H. JOHNSON: *Phys. Rev.*, **83**, 510 (1951).

([7]) K. A. BRUECKNER, R. SERBER and K. M. WATSON: *Phys. Rev.*, **84**, 258 (1951).

([8]) R. BIVINS, N. METROPOLIS, M. STORM, A. TURKEVICH, J. M. MILLER and G. FRIEDLANDER: *Bull. Am. Phys. Soc.*, **2**, 63 (1957).

([9]) T. FUJII: to be published. The writer is indebted to Mr. FUJII for the use of his results before publication.

2. – Energy sensitive detectors.

A Čerenkov counter was used as an energy sensitive counter (ESC) by pulse height analyzing its output ([10]). If the entire range over which a pion can produce Čerenkov light be within the radiator of the counter, more light is produced with increasing energy because of the longer path as well as because of the increased radiation from the greater velocity. Because the Čerenkov counter counts only charged particles whose velocity is greater than the velocity of light in the radiator material, it rejects nucleonic background. When used with a pulse height analyzer, the Čerenkov counter has the additional advantage of simultaneously recording events over the entire part of the energy spectrum for which Čerenkov light is produced. The disadvantages of the Čerenkov counter include small light output, causing a noise problem; a pulse height spectrum that is not simply related to the energy spectrum; and instrumental complexity. In spite of these difficulties, energy resolution on the order of ± 7 MeV was obtained over the energy range of $115 \div 150$ MeV in these experiments. A Čerenkov counter of this type is limited at low energies where little or no Čerenkov light is produced, and loses its energy sensitivity at high energies because the range over which a pion can produce Čerenkov light becomes longer than the radiator.

In the energy range below the Čerenkov threshold, a scintillation counter was used by pulse height analyzing its output. Energy resolution of $\pm 15 \div 20$ MeV was obtained. The scintillator does not share the ability of the Čerenkov counter to discriminate pions over nucleonic background, but since the light output is much larger the noise problem is not severe. When used with negative pions, the scintillator light output varies widely from pion to pion because charged star products following pion capture after the pions come to rest contribute to the total light output. For this reason the scintillator should be much easier to use with positive pions, for which this type of capture does not occur. Both the Čerenkov and scintillation counters have high counting efficiencies.

In contrast, the type of detector used by RAINWATER *et al.* ([4]) uses two scintillation counters with sufficient absorber between them to accept only pions with energy near that of the incident beam. This method has the advantage of simplicity, but straggling limits the accuracy of energy determination, and absorption and scattering in the absorber limit the counting efficiency. RAINWATER *et al.* ([4]) report energy resolution of $\pm 15 \div 20$ MeV for 80 MeV

([10]) J. R. WINCKLER, E. N. MITCHELL, K. A. ANDERSON and L. PETERSON: *Phys. Rev.*, **98**, 1411 (1955).

pions. The energy resolution of a detector of this type must be limited to obtain a satisfactory counting efficiency. At higher energies, poorer energy resolution is expected because of the additional range straggling. By using a third counter in anticoincidence behind the second counter, this method can be extended to energies below that of elastic scattering. A modification of the method using two counters with absorber between them is the method which demands a coincidence with the muon from decay of a pion brought to rest in the second counter ([11]). This method is not applicable to the counting of negative pions because of capture processes. An alternative possibility would be a magnetic spectrometer. It has the advantage of measuring the differential energy spectrum directly, both for elastic and inelastic scattering. The use of an existing magnet was considered which was estimated to have an energy resolution of ± 8 MeV at 150 MeV with a solid angle of 0.014 steradian. This solid angle is much smaller than that obtainable with counters, and would require much more intense pion beams to compete with the Čerenkov and scintillation counters with a pulse height analyzer. In principle the magnetic spectrometer affords the best energy resolution for studying elastic scattering with high angular definition, but it is not as well suited to the measurements of energy spectra for the inelastic scattering. The magnetic spectrometer and absorber counter methods might be extended to measure an entire energy spectrum simultaneously, but the instrumentation required is as complex as that for the pulse height analysis (PHA) method.

In these experiments the PHA method was used. The number of counts in a PHA channel represents an integral over energy of the unknown energy spectrum multiplied by the probability that a pion of given energy will produce a pulse in that channel. It is necessary to unfold the PHA's to give the required energy spectrum. Because of the width of the probability function, poor statistical use is made of the counts in the determination of energy spectra. The probability function, or calibration, is determined by making a PHA of the ESC output with monoenergetic beams at each of several different energies. The calibration includes the effects of straggling and absorption of the pions, statistics of the photoelectrons, and charged star products in the scintillator.

The ESC's had tapered sensitive elements to improve the light collection by internal reflection. The amount of taper was determined by the area of target illumination and the distance from the target at which the counter was to be operated. A pair of scintillation counters was mounted with the ESC to define the solid angle and to produce a gating pulse for the pulse height analyzer. For the Čerenkov ESC's, the radiators were made as long as the

([11]) See, for example, W. IMHOF: *University of California Radiation Laboratory Report UCRL-3833* (1956).

range over which a 150 MeV pion can produce Čerenkov light. Measurements at various angles were made by moving the ESC.

At forward angles, the tapered lucite counter, which had a cast lucite Čerenkov radiator 18 inches long tapering from 2 inches to 5 inches, was used. A 5 inch DuMont photomultiplier (Type 6364) was fitted to the larger end. This counter was operated 24 inches from the target and had a solid angle of 0.0055 steradian with an angular half width of 3°.

For scattering beyond 45° a larger counter, which had an angular half width of 11° and a solid angle of 0.12 steradian when operated 14 inches away from the target, was used (Fig. 1). The sensitive element of this counter was

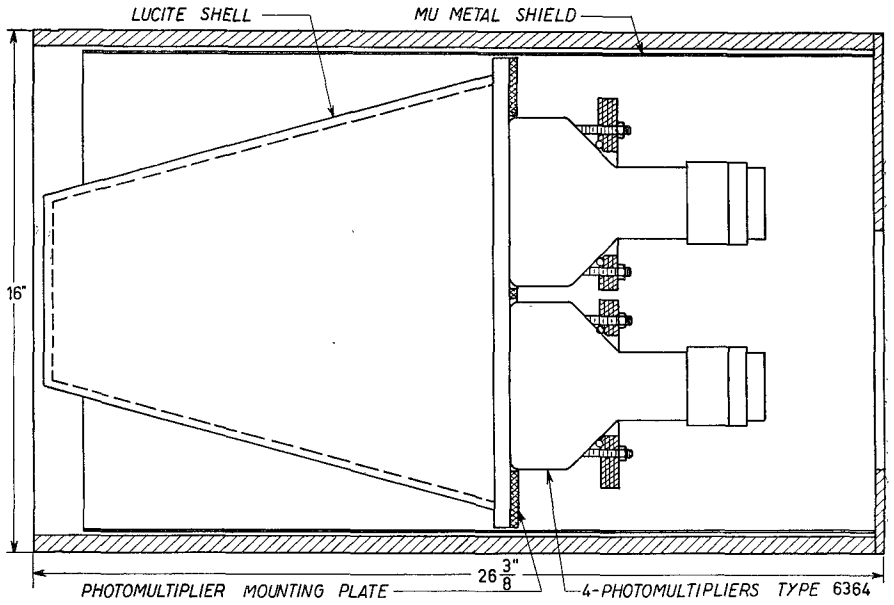

Fig. 1. – Large liquid counter.

17 liters of liquid contained in a lucite shell 14 inches long and tapering from $5\frac{7}{8}$ to $13\frac{5}{8}$ inches. The larger end was fitted with four DuMont 5 inch photomultipliers. For use as a Čerenkov counter, the shell was filled with a mixture of distilled water and 10 mg/l of light shifter, DuPont coompund MDD 3169 ([12]). For use as a scintillator, the shell was filled with a mixture of phenylcyclohexane with 3 g/l of PBD ([13]). This counter is referred to hereafter as the « liquid Čerenkov » or the « scintillator » according to its filling.

([12]) E. HEIBERG and J. MARSHALL: *Rev. Sci. Instr.*, **27**, 618 (1956).

([13]) F. N. HAYES, D. G. OTT, V. N. KERR and B. S. ROGERS: *Nucleonics*, **13**, No. 12, 38 (1955); F. N. HAYES, D. G. OTT and V. N. KERR: *Nucleonics*, **14**, No. 1, 42 (1956).

3. – Experimental arrangement.

The meson beam produced by the cyclotron was brought through a strong focus lens and the rotary shield to the experimental area, where it was deflected by a wedge magnet to select a beam of (150 ± 6) MeV negative pions (14) (Fig. 2). The pion beam had an intensity of $5 \cdot 10^5$ per minute time

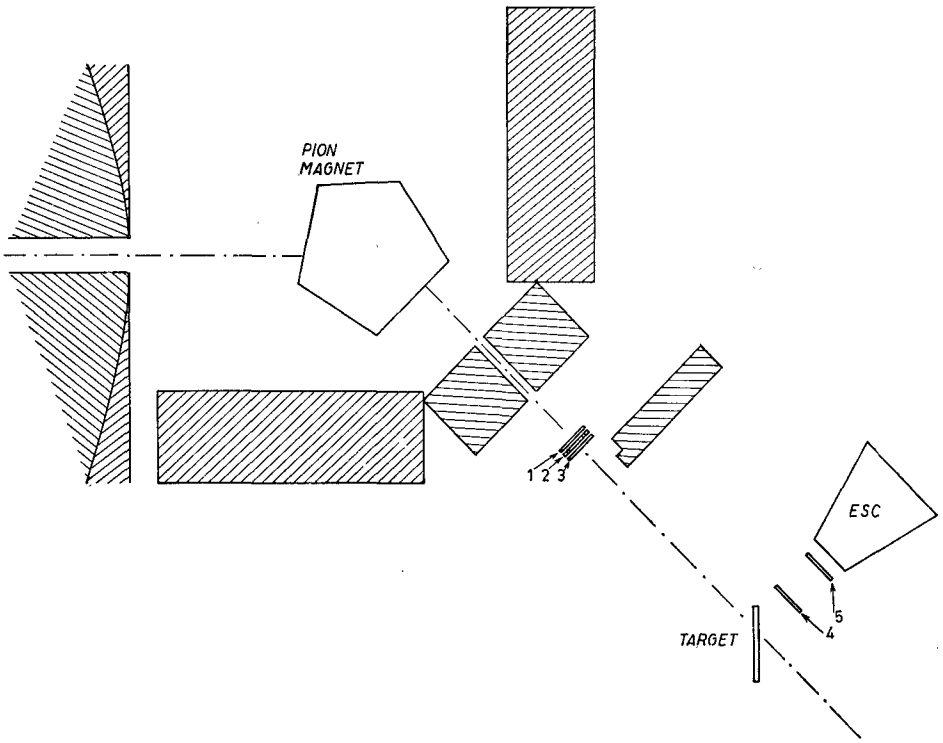

Fig. 2. – Experimental arrangement. The sandwich of beam monitoring counters is 1, 2 and 3. ESC is the energy sensitive counter. The gating counters mounted with the ESC are 4 and 5. Shielding is shaded.

average with a duty factor of 180. Muons and electrons contaminated the beam by (8 ± 1) percent. The beam was circular in profile with a radial dependence which was roughly Gaussian with a $1/e$ radius of 1 inch and angular spreads of ± 1° vertically and horizontally. The incident pions were estimated to have an rms energy spread of 3 MeV. Lower energy beams for the calibration of the energy sensitive counters were obtained from the 150 MeV beam by

(14) S. WARSHAW and S. C. WRIGHT: to be published.

the use of absorbers. For this purpose, the absorbers were placed between the cyclotron and the wedge magnet, so that the magnet would remove muons from the incident beam and would reduce the energy broadening by range straggling in the absorber.

The incident beam was monitored by a sandwich of three scintillation counters, one of which used spots of scintillator to cover about 1/12 of the beam area to reduce the counting rate to allow reliable scaling. The partial counter was not included in the multiple coincidences for gating purposes. The coincidence circuits used where similar to those described by ANDERSON *et al.* ([15]) as modified by DAVIDON and FRANK ([16]).

Pulses from the energy sensitive counters (ESC's) were stretched at the counters, then amplified in linear amplifiers and sent to a 100 channel pulse height analyzer ([17]). This pulse height analyzer will accept pulses approximately 400 microseconds apart, so will accept only one pulse per cyclotron beam burst. It has a quoted stability of 0.1 percent. The circuits used in the pulse height analyzer are of standard design and need pulses of about 1 microsecond length, and amplified to about a 100 volt peak level. The pulse height analyzer can be gated to accept pulses in coincidence with other counters. The analyzer was gated by a fast quadruple coincidence ($\sim 2 \cdot 10^{-8}$ s) of two counters in the beam monitoring sandwich and the two gating counters mounted with the ESC's. The quadruple counts were recorded, as were the quintuples resulting from a fast coincidence of the quadruples with a clipped output of the ESC. The quadruples count records the sum of the elastic and inelastic scattering.

The angles at which each ESC was used and the average counting rates with the various targets are given in Table I. The counting rates refer to the quintuples count which differs slightly from the total count in the pulse height analyzer because of accidental counts in the analyzer and different threshold levels for the analyzer and the quintuples coincidence circuits. Each time an ESC was set up at an angle, pulse height analysis (PHA) runs were made with the carbon and lead targets, and a PHA run was made with no target. The target-in target-out difference was attributed to scattering from the target. Each time the angle was changed, the ESC was returned to the in-line position to check drifts in the PHA calibration before setting up a new angle. All angular measurements were repeated to check the consistency of the data. The various angles were set up to $\pm 1°$. To estimate the accidentals in the PHA, the PHA of the ungated singles of the liquid ESC with the cyclotron

---

([15]) H. L. ANDERSON, M. GLICKSMAN and R. L. MARTIN: *Proceedings of the National Electronics Conference*, **9**, 483 (1953).

([16]) W. DAVIDON and R. FRANK: *Rev. Sci. Instr.*, **27**, 15 (1956).

([17]) Model PA-3; Pacific Electro-Nuclear Company, Culver City, California.

TABLE I. – *Counting rates (counts per minute, time average).*

Counter angle		Target				
(Note [1])	(deg)	1 in. C	½ in. C	¼ in. Pb	⅛ in. Pb	None
T. L.	18.5	146	91	252	115	27
T. L.	24	97	58	76	37	12
T. L.	31	56	28	29	15	4.3
T. L.	36.5	28	15	14	6.3	2.2
T. L.	44	13	6.4	6.9	3.6	0.75
Ck.	45	230	127	100	41	4.3
Ck.	60	46	24	42	—	0.34
Ck.	75	30	20	20	7.5	0.25
Ck.	90	41	22	24	—	0.35
Ck.	115	33	11	10	5.1	0.34
Ck.	138	22	11	8.7	5.3	0.22
Sc.	45	266	—	113	—	6.9
Sc.	90	185	—	67	—	1.3
Sc.	138	200	—	100	—	2.5

[1] T. L. = Tapered lucite counter; Ck. = Liquid Čerenkov counter; Sc. = Liquid scintillation counter.

beam on was run at each angle. Checks on the voltages of the photomultipliers and on the gain of the amplifier system through the pulse height analyzer were run each time an angle setup was made.

A transmission measurement was made to determine the attenuation cross-sections for both carbon and lead. The mean half angle subtended by the transmission counter at the target was 25°. The integrated elastic cross-section was subtracted from the attenuation cross-section to determine the total cross-section for inelastic processes. By subtracting the integrated cross-section determined from the quadruples counts from the attenuation cross-section, the sum of the absorption and charge exchange cross-sections was determined.

4. – Pulse height analyses.

Typical calibration curves for the liquid Čerenkov counter are shown in Fig. 3. The experimental points of a typical run are shown compared to one of the curves. The errors shown are due to counting statistics alone. The broad peak is interpreted as the distribution of pulse heights arising from the statistics on the photoelectrons and straggling at the end of the range over

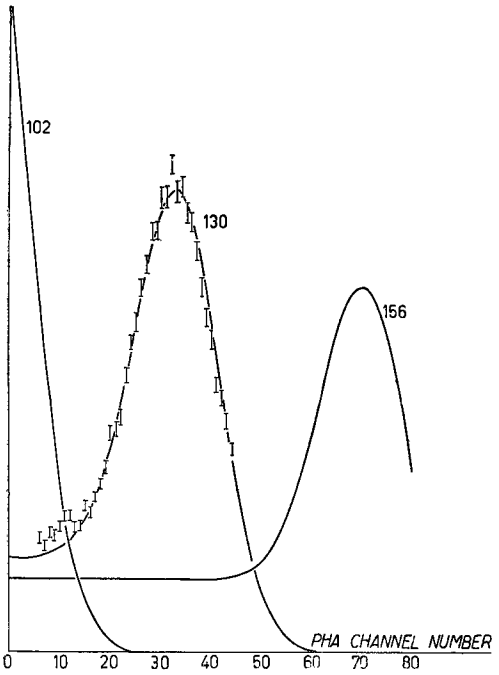

Fig. 3. – Smoothed calibrations for liquid Čerenkov energy sensitive counter. Number of counts per channel vs. channel of the pulse height analysis, for 3 different monoenergetic pion beams at 102, 130, and 156 MeV. An experimental calibration at 130 MeV is shown for comparison.

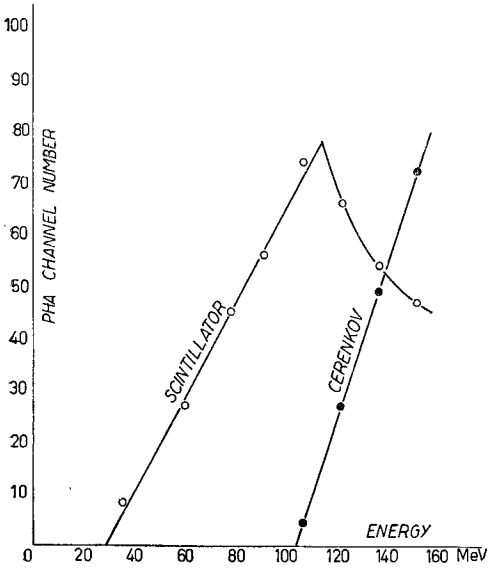

which the pions can produce Čerenkov light. A long tail extending toward the smaller pulses is presumed to arise from the nuclear encouters of some of the pions before they reach the end of the Čerenkov range. From the width of the peak, it is inferred that 100 to 200 photoelectrons are collected for a pulse at 150 MeV. About 270 photoelectrons were expected assuming 0.1 probability per quantum to produce a photoelectron and 0.5 light collection efficiency. The channel of the pulse height analysis (PHA) in which the peak appears is very nearly a linear function of the energy (Fig. 4). The shape of the PHA's at various energies is very similar if expressed as a function of the channel relative to the peak. The Čerenkov counter is assumed to produce a pulse for every pion which enters it, so its efficiency at any given energy is the probability that the pulse falls within the range of the PHA. The gating counters mounted with the energy sensitive counters (ESC's) served to assure that most of the pions would not escape through the side walls of the counter; this was borne out in the off center beam tests of the counters. The contri-

Fig. 4. – Channel of the pulse height analysis in which the peak of the calibrations appears for various energies of monoenergetic calibration beams, for the scintillation counter and liquid Čerenkov counter.

bution of muons to the calibration curve is a separate peak of larger pulses which has been removed from Fig. 3. The calibration curves for the two Čerenkov counters are quite similar, so only those for the liquid Čerenkov are shown.

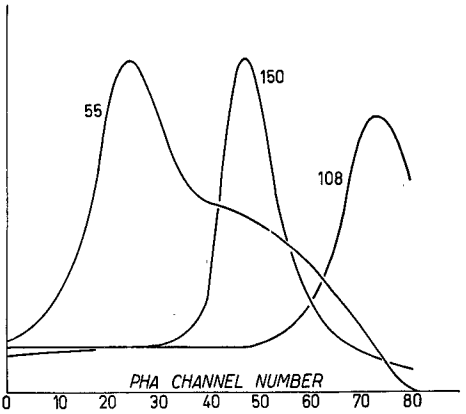

Fig. 5. – Calibrations for liquid scintillation energy sensitive counter for 3 different monoenergetic pion beams at 55, 150, and 108 MeV. At 150 MeV, pions travel all the way through the scintillating material without stopping.

For energies at which a pion stops within the scintillator (less than 107 MeV), the calibration curves from the energy sensitive liquid scintillator are quite similar to those of the Čerenkov, except for a shoulder on the large pulse side of the peak (Fig. 5). This shoulder is interpreted as arising from charged star products from pion capture in the scintillator material. The scintillator calibrations are not much narrower than those of the Čerenkov in spite of the greater light collection, because of straggling and the energy width of the calibrating beams. For these energies, the channel of the PHA in which the peak appears is very nearly a linear function of the energy (Fig. 4). The curve does not extend to the origin because a pion must have sufficient energy to traverse the gating counters and the front wall of the liquid counter before it can reach the scintillator fluid, and because of the threshold operation in the pulse height analyzer. A break in the curve of the channel of the peak as a function of energy appears at higher energies, where a pion can travel all the way through the scintillator. The amount of light produced then decreases with increasing energy, because of the smaller ionization of the more energetic particles. The characteristic shoulder on the large pulse side of the peak diminishes with increasing energy because the capture and resultant star formation are reduced. This shoulder is not noticeable at 150 MeV. Because the energy analysis cannot separate the contributions of energies above and below the knee, the contribution of the energies above the knee must be subtracted. For this purpose, data from the Čerenkov counter runs were used in conjunction with the calibrations run on the scintillator at these higher energies.

Both of these energy sensitive counters had a drift in the channel in which the peak of the calibration appeared at a given energy. The drift was probably a gain drift in the photomultipliers. For the purposes of this experiment, the effect was corrected by taking frequent calibration runs and recording the position of the peaks at any given time. This record made it possible to deter-

mine the energy belonging to any particular channel of the PHA to within $1 \div 2$ MeV at any time during the runs.

Fig. 6 shows typical PHA's which had to be energy analyzed to give the plots of cross-sections as a function of energy. The actual PHA is not a smooth curve as shown, but consists of a point at each channel number with random variations due to counting statistics in each. The curves shown were drawn through the middle of the spread of these points. Most of the sharp rise toward the low end of the PHA for carbon at 90° in the Čerenkov counter is due to accidental counts. An energy analysis of these accidentals was made by subjecting a PHA of ungated singles in the pulse height analyzer to the same energy analyzing process as was used on the angular data. Ninety percent of the ungated singles from the liquid Čerenkov counter appeared in the energy analysis at around 102 MeV, the lowest energy tabulated. Because of the large fraction of accidental counts present, the lowest energy values from the liquid Čerenkov counter beyond 60° are not regarded as reliable.

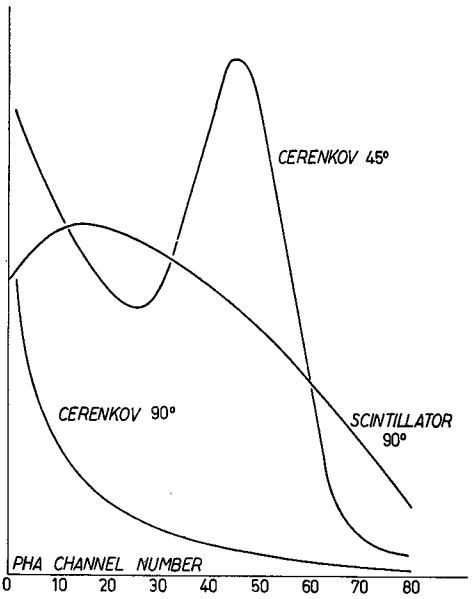

Fig. 6. – Pulse height analyses run with a carbon target at 45° and 90° with the liquid Čerenkov counter, and at 90° with the liquid scintillation counter.

5. – Energy analysis process.

The results which are required of the energy sensitive counter (ESC) are the number of events occurring at some energy E. The energy analysis (EA) process described takes a pulse height analysis (PHA) run at a given angle with a given target and converts it into an energy spectrum at that angle. The least squares method used cannot produce a continuous spectrum, but gives a histogram of the number of events, a_j, associated with each of several energies, E_j.

The ESC sees a « true » number of counts, m_ν (in the statistical sense), in channel ν of the PHA. The actual number of counts in channel ν, M_ν, approximates to m_ν, and is assumed to differ only because of the finite sampling. M_ν is accordingly Poisson distributed about m_ν, and the limit in which M_ν can be treated as normally distributed is considered. If necessary, channels of the PHA are grouped to assure that M_ν can be treated as normally

distributed. Averaging over the energy dependences of the cross-sections as smeared out by the energy changes of a pion within the target and considering only single encounters, m_ν is given by:

$$m_\nu = \int \mathrm{d}E\, K_\nu(E) \int_{\text{Target}} \mathrm{d}V\, N(\boldsymbol{x})\, I(\boldsymbol{x}) \int_{\text{Counter}} \mathrm{d}A\, \frac{\cos\delta}{r^2}\, \frac{\mathrm{d}^2\sigma}{\mathrm{d}\Omega\, \mathrm{d}E} = \int \mathrm{d}E\, K_\nu(E)\, q(E)\,,$$

where E is the energy at which the pion leaves the target, $N(\boldsymbol{x})$ is the number of scattering centers per cm³ in the target at position $\boldsymbol{x}$, $I(\boldsymbol{x})$ is the number of pions per cm² at position $\boldsymbol{x}$ integrated over the time of the run, $\boldsymbol{r}$ is the vector from the volume element $\mathrm{d}V$ at $\boldsymbol{x}$ in the target to the element of area $\mathrm{d}A$ on the counter, $\cos\delta$ is the cosine of the angle formed by $\boldsymbol{r}$ and the normal to $\mathrm{d}A$, $K_\nu(E)$ is the probability that a pion of energy E will produce a pulse in channel ν of the pulse height analyzer, and $\mathrm{d}^2\sigma/\mathrm{d}\Omega\,\mathrm{d}E$ is the cross-section sought. There is a simi ar equation for each channel of the PHA, so the problem is to find a solution, $\mathrm{d}^2\sigma/\mathrm{d}\Omega\,\mathrm{d}E$, which is consistent with a large number of equations. The volume and area integrations reduce in lowest order to

$$q(E) = A(\theta)\, T_{123}\, \frac{\mathrm{d}^2\sigma}{\mathrm{d}\Omega\, \mathrm{d}E}\,,$$

where $A(\theta)$ is the coefficient resulting from the evaluation of the integral and T_{123} is the corrected number of monitor counts. $A(\theta)$ includes the corrections arising from turning the target to half the angle of the counter and other corrections listed in detail in Sect. **6.**

To calibrate the counter, $q(E)$ is replaced by a spectrum which is non-zero only in some small region near E_j

$$m_\nu \approx K_\nu(E_j) q(E) \Delta E\,; \qquad K_\nu(E_j) \approx \frac{M_\nu}{q(E)\Delta E} = A_{\nu j}\,.$$

The use of different energies E_j results in a (non-square) matrix $A_{\nu j}$ which approximates to the set of continuous functions $K_\nu(E)$. The $A_{\nu j}$ are referred to as calibrations. Each ESC has its own set of calibrations.

For the measurements runs, an approximate solution can be obtained in the form

$$m_\nu \approx \sum_j A_{\nu j} q(E_j) \Delta E_j = \sum_j A_{\nu j} a_j\,.$$

The reduction to this form is immediate if the energy spectra of the $A_{\nu j}$ and the a_j are regarded as histograms with the blocks of the histogram centered at (equidistant) energies E_j. If the energy spectrum of the $A_{\nu j}$ and the a_j be regarded as « trapezoidal » (linear interpolations between the values at E_j),

there exists a non-singular linear transformation of the amplitudes which satisfies the above equation. The histogram approximation and the trapezoidal approximation thus contain equal amounts of information, so the simpler histogram approximation is used.

The actual number of counts in a channel of the pulse height analyzer, M_ν, is not exactly equal to the « true » number m_ν, so a statistical method of reduction must be used. The method used in reducing the raw data is similar to the « modified χ^2-minimum method » ([18]). The essential features of this method are the reduction of the statistical variables to mean zero and unit standard deviation, and the subsequent solution of the problem by a least-squares method. Accordingly a function

$$\chi^2 = \sum_\nu \frac{(M_\nu - m_\nu)^2}{\Delta_\nu^2} ,$$

is formed. It is assumed in this form of writing that the various channels of the PHA are independent. The Δ_ν^2 are the variances of the counts in channel ν of the PHA. Differentiating χ^2 by a_j, it is found that the solution to the problem can be written in the form

$$a_j = \sum_k (G^{-1})_{jk} C_k$$

$$C = \sum_\nu \frac{M_\nu}{\Delta_\nu^2} A_{\nu k} ;$$

$$G_{jk} = G_{kj} = \sum_\nu \frac{A_{\nu j} A_{\nu k}}{\Delta_\nu^2} .$$

The amplitudes a_j can thus be found by inverting the matrix G. The a_j so found are correlated random variables whose means are the values given and whose moment matrix is G^{-1} ([19]). This method is the same as the maximum likelihood method usually used in reducing experimental data in the limit where the data are normally distributed instead of Poisson distributed.

The measured number of counts in channel ν of the pulse height analyzer, M_ν, was taken as the difference of the target-in and target-out counts in channel ν; $M_\nu = D_\nu - B_\nu$. Δ_ν^2 was estimated as $D_\nu + B_\nu$. This estimate of Δ_ν^2 from the measured value rather than from the calculated estimate is an approximation in the method that is valid when the data are normally distributed. The approximation has the consequence that Δ_ν^2 is not dependent on the a_j and thus makes no contribution to the differentiation by a_j. This makes

([18]) H. CRAMÉR: *Mathematical Methods of Statistics* (Princeton, 1951), Sect. 30.3.

([19]) F. SOLMITZ: *Notes of the Least Squares and Maximum Likelihood Methods* (unpublished).

the algebraic process linear and is the feature that makes the method similar to the « modified χ^2-minimum method ». Measurement errors in the A_{vj} are not included in estimating Δ_v^2.

The value of χ^2 can be obtained by observing that

$$\chi^2 = \sum_v \frac{M_v^2}{\Delta_v^2} - \sum_j a_j C_j .$$

This provides a check on the calculations.

The problem must be completely redone for each target and angle because the matrix G is different for each set of data.

This problem has been coded for the AVIDAC electronic computer at the Argonne National Laboratory. The AVIDAC was given the A_{vj}, the D_v, and B_v; it then calculated the matrix G, inverted G, checked the inversion, calculated C_j and evaluated a_j and $\sum_v M_v^2/\Delta_v^2$ from which the χ^2 estimates were made.

The errors quoted on a_j from the energy analysis are the square roots of the diagonal elements of the moment matrix and have the following meaning: If one of the elements a_j be changed by the amount indicated, *and* the corresponding changes induced by the correlations be made in the remaining elements, the value of χ^2 will be increased by one. Any other combination of changes in the elements of a_j will cause more rapid changes in χ^2.

In some cases, the pulse height analysis had other components added to the count in channel v. Examples arose with 1) accidental counts in the Čerenkov counter; 2) protons in the scattered pion beams counted by the scintillator; 3) electrons from converted γ-rays from the decay in the target of charge exchange π^0's; and 4) the scintillator where the higher energies produced PHA's which could not be analyzed directly because of their similarity to the lower energy components. The subtraction process described here was used to obtain the corrected EA's in these cases. In each case the argument is formally the same, so it is given for the case of the scintillator subtractions only. The integral over energy is broken into two parts, above and below the knee of the channel of the peak vs. energy curve (Fig. 4). Each integral can then be replaced by a sum as before, with the result

$$m_v = \sum_j A_{vj} a_j + \sum_k P_{vk} p_k ,$$

where the P's and p's mean the same thing as the A's and a's, but refer to energies above 107 MeV. The p_k are known amplitudes determined from the Čerenkov energy analysis of the same target at the same angle. Let P_{vk} be represented as

$$P_{vk} = \sum_j A_{vj} S_{jk} ,$$

by an EA process identical to that used for the a_j previously, so

$$m_\nu = \sum_j A_{\nu j}(a_j + \sum_k S_{jk} p_k) .$$

There are now correlations between the various channels of the PHA which are induced by the determination of the subtraction amplitudes. The form for the problem is

$$\chi^2 = \sum_{\mu,\nu} H_{\mu\nu}[M_\mu - m_\mu][M_\nu - m_\nu] ,$$

where $(H^{-1})_{\mu\nu} = \Delta_\nu^2 \delta_{\mu\nu} + \Gamma_{\mu\nu}$ is the moment matrix of $[M_\mu - m_\mu]$; Δ_ν^2 is the (diagonal) moment matrix of the measured values, M_ν; $\Gamma_{\mu\nu} = \sum_{j,k} P_{\mu j} P_{\nu k} \overline{\Delta p_j \Delta p_k}$; and $\overline{\Delta p_j \Delta p_k}$ is given by the moment matrix of the energy analysis of Čerenkov data which yields the p_k. By direct evaluation some of the larger elements of $\Gamma_{\mu\nu}$ were 1-2; while some of the smaller off-diagonal elements ran down to 0.1 or less. All elements evaluated were positive. Since the Δ_ν^2 were around 200 for these same places, the $\Gamma_{\mu\nu}$ were ignored by comparison. The weighting for the various channels is thus that given directly by the measurements, so the same EA routine can be used whether or not the subtractions are present. The subtraction is then done in the EA, energy-by-energy. For the application to the scintillator subtraction process, the Čerenkov data must be multiplied by the ratio of the energy intervals between the energies of the scintillator EA to those of the Čerenkov EA.

In the actual EA, smoothed calibrations were used. It was found that the calibrations could be expressed as a function of the channel relative to the channel of the peak for the energy in question

$$A_{\nu j} = N_j F(\nu - \nu_j) ,$$

where N_j is a normalizing coefficient, ν is the (variable) channel of the PHA, and ν_j denotes the channel in which the peak of the pulse height distribution appears at energy E_j. For the function $F(\nu - \nu_j)$ a form suggested by the experimental calibrations was used. Thus, for the liquid Čerenkov counter, $F(\nu - \nu_j)$ was a Gaussian of 10-channel half width above and below ν_j with a constant number $\frac{1}{5}$ of the peak value added to all channels $\nu < \nu_j$. For the scintillator, $F(\nu - \nu_j)$ was tabulated from a curve obtained by smoothing the averages of calibrations for 5 different energies. A χ^2-test applied to the scintillator calibrations thus obtained indicated that on the average $F(\nu - \nu_j)$ differed from the measured values by 2 standard deviations; one standard deviation is the expected value if $F(\nu - \nu_j)$ describes the situation perfectly. This method of forming the calibrations was not used on the tapered lucite

counter where the experimental calibrations (apart from a normalization dependent upon the energy) were used directly.

6. – Calculations.

In all, some 85 energy analysis (EA) calculations were run for the three counters at the various angles with the various targets. The separate runs with the same angle, target, and energy sensitive counter (ESC) were combined where possible. In each case a plot of the 5-channel sums of the pulse height analysis (PHA) was made to verify the agreement of the broad features of the PHA before making the combination. The entire PHA for a target and angle was grouped in 5-channel sums if the raw data had fewer than 10 counts in each of several channels. Grouping was done in this way to avoid giving more weight to one part of the pulse height spectrum than to another. All the tapered lucite data were grouped into 5-channel sums because the calibrations did not seem to justify the retention of the full number of channels. Eighty channels of PHA data were retained, thus all EA's had either 80 or 16 input channels.

The nature of the PHA's to be reduced is shown in Fig. 6. Some typical EA's and moment matrices as printed out by the computer before the subtractions were made are given in Tables II to IV. These EA's are scaled to represent the actual number of pions in the various energies. The correlations, given by the off-diagonal elements of the moment matrix divided by the square

TABLE II. – *Matrix and vector for Čerenkov energy analysis for carbon target at* 90°. $\chi^2 = 67$. (Expectation is 74).

Energy	155	145	134	124	114	103
Vector	387	270	858	1468	1821	8633
Matrix	5611	−4109	1660	−1342	583	−1098
		8061	−5189	2825	−2102	2496
			9184	−7038	4684	−6299
				13990	−12283	15326
					26537	−41041
						121119

root of the product of the two diagonal elements each connects, are quite large. Thus for calculations of derived quantities involving more than one energy, the error estimates may be quite different from those shown on the plots.

The number of energies into which the PHA can be energy analyzed is a

TABLE III. – *Matrix and vector for scintillator energy analysis into 6 energies for carbon target and 90°.* $\chi^2=115$.

Energy	109	95	77	61	44	28
Vector	18	2446	2758	24 9	5304	6031
Matrix	61730	−45410	−13740	7073	23477	−24405
		84565	−35694	−10185	−1206	13314
			96097	−50835	−17259	22574
				101275	−51486	2918
					134643	−93780
						103883

TABLE IV. – *Matrix and vector for scintillator energy analysis into 5 energies for carbon target at 90°.* $\chi^2 = 145$.

Energy	110	90	69	49	28
Vector	280	3368	2931	5334	7293
Matrix	49765	−35779	−10344	26757	−19368
		71554	−35980	−16390	23200
			76860	−43605	8653
				94912	−63014
					71448

compromise between trying to get as many energies as possible and troubles in the calculation arising from difficulty in inverting the matrices. This feature of the practical calculation places a limit on the energy resolution obtainable from the ESC's in addition to those limitations inherent in the counter itself. The matrices from full 80 channel calculations were easier to invert than those from the calculations with the 5-channel sums. There seems to be no simple criterion to determine the number of energies into which the data may be analyzed.

Neither the energy spread of the calibrating beam nor the energy broadening of the elastically scattered pions by straggling and by different path lengths through the target had any systematic effect on the energy analysis. They contributed to the uncertainty in the energy determination without affecting the amplitudes.

In the calculations of cross-section, corrections were applied for certain systematic effects. These corrections were included in the factor $A(\theta)$ of Sect. 5. A geometrical correction was applied for the different number of effective scatterers as the target was turned to bisect the angle between the beam and

the ESC. The pion decay in flight between the target and the ESC was about 4 percent for the higher energy pions. The correction for the attenuation of the incident beam in the target varied from 2 to 5 percent with the target and angle. About 2 percent of the pions going to the ESC were scattered out or absorbed in the first counter of the gating pair mounted with the ESC and did not contribute to the quadruples count. An additional 3 percent were scattered out or absorbed before entering the ESC. The muon and electron contamination of the beam was around 8 percent, while the contribution to the total count of muons Coulomb scattered by the target was less than 1 percent at all angles. The geometrical corrections for the finite size of the counter used by ANDERSON *et al.* [20] could not be applied here because it is not possible to make the assumptions about smoothness of the cross sections which can be made in the case of scattering by hydrogen. The magnitude of these corrections was estimated and found to be largest for the elastic scattering, where it was around 5 percent. The large counter size may account for the possible loss of some features of the elastic scattering, such as diffraction minima, but it was not expected to obscure the general features of the inelastic scattering.

Plural inelastic scatterings do not appear within the experimental accuracy. With lead at angles less than 30°, corrections for multiple Coulomb scattering were made by the method of MARTIN [21].

Corrections which must be applied through the use of the subtraction process described in Sect. 5 include those for spurious counts in the ESC's caused by nucleons and γ-rays from absorptions or charge exchange events. A proton must have energy near 70 MeV to record in the counter. The cross-section for production of a proton of $E > 70$ MeV by a 150 MeV negative pion is about 1/20 geometrical and is somewhat forward peaked [22-24]. Estimates of the energy spectrum of these protons indicated that almost all proton pulses in the scintillator would appear in the lowest energy of the EA. The protons made a contribution to the measured differential cross-sections at 90° of about 1 mb/sr for carbon and 10 mb/sr for lead. A correction for this was applied to the cross-sections from the quadruples counts and to the lowest energy of the scintillator EA. The neutron counts were negligible. The expected PHA of electrons from the conversion of π^0 γ-rays would energy analyze

---

[20] H. L. ANDERSON, W. DAVIDON, M. GLICKSMAN and U. E. KRUSE: *Phys. Rev.*, **100**, 279 (1955).

[21] R. L. MARTIN: *Phys. Rev.*, **87**, 1052 (1952).

[22] G. BERNARDINI, E. T. BOOTH, L. LEDERMAN and J. TINLOT: *Phys. Rev.*, **82**, 105 (1951); G. BERNARDINI, E. T. BOOTH and L. LEDERMAN: *Phys. Rev.*, **83**, 1075 (1951); G. BERNARDINI and F. LEVY: *Phys. Rev.*, **84**, 610 (1951).

[23] A. H. MORRISH: *Phys. Rev.*, **90**, 674 (1953); *Phil. Mag.*, **45**, 47 (1954).

[24] A. TURKEVICH: Private communication.

into a distribution peaking at the top energy of the Čerenkov counter. In the scintillator, the electrons would contribute to some of the lower energies. In lead the correction for the γ-rays of π^0 decay was about 5 mb/sr and in carbon the correction was negligible. These corrections, estimated from the high-energy parts of the energy analysis at backward angles, are in agreement with the corrections expected from the charge exchange cross-sections reported by LEDERMAN *et al.* [3].

Because the histogram approximation has been used in the energy analysis, the ordinates of the plots of energy dependent cross-sections are the height of a histogram block which extends 5 MeV above and below the point plotted. Where a curve is drawn through the plotted points, this curve is the locus of the top center of a histogram block.

The errors shown in the plots of energy dependent cross-sections are determined from the diagonal elements of the moment matrices and the error estimates of the coefficients for the reduction of the EA's to energy dependent cross-sections. Errors in the coefficients affect all energies in the same way and are properly represented by a moment matrix. The final moment matrix is the sum of the two. The energy dependent cross-sections in the $120 \div 150$ MeV range of the Čerenkov are correlated to those in the $60 \div 100$ MeV range of the scintillator at a given angle because of the subtraction. The values in the $60 \div 100$ MeV range at 45° are quite uncertain because of the large elastic scattering at this angle.

There is a negative region in the EA's of the scintillator data at 138° for both carbon and lead which probably results from a faster decrease of count with increasing PHA channel number that can be constructed with the calibrations. The best fit is obtained from the available calibrations with a large value at low energies and a negative value at higher energies to bring the counts down rapidly with increasing channel number. The experimental calibrations at very low energies ($\sim$10 MeV) had this type of rapid drop-off of count with increasing PHA channel number. A negative region thus implies that most of the pions counted were at an energy even lower than the lowest energy of the EA.

Elastic cross-sections have been determined where possible as the area under the elastic peak. Where a peak is not clear, an upper limit can be set on the amount of elastic scattering. This limit is usually quite small. In carbon at 138°, the elastic cross-section is less than about 0.5 mb/sr, while for lead at the same angle the elastic cross-section is less than about 2 mb/sr.

The cross-sections determined from the quadruples counts are not reliable at extreme forward angles ($\cos\theta \gtrsim 0.9$) because of the decay of part of the incident pion beam between the deflecting magnet and the target, which produces muons at a slight angle to the beam that can multiple scatter into the counters at forward angles. The Čerenkov counter did not respond to these

muons because of their low energy. The muon energy is low because those muons which contribute are those at the extreme angles, which come off slightly backwards to the pion motion, so have velocity less than the pion velocity and energy around 100 MeV. Order-of-magnitude estimates indicate that 10 percent of the quadruples counts at 18.5° in lead were multiply scattered muons. These muons do not affect the calculation of the absorption plus charge exchange cross-section determined by subtraction of the integrated quadruples cross-section from the attenuation cross-section, because the muons were counted by the transmission counter used in the determination of the attenuation cross-section.

7. – Monte Carlo calculations.

Quasi-elastic scattering, in which the scattering of pions by complex nuclei is described as the result of incoherent scattering by individual nucleons, can be calculated by the Monte Carlo method ([6-8-25]). Monte Carlo calculations were run on the MANIAC electronic computer at the Los Alamos Scientific Laboratory for comparison with the present experimental results, using the calculation coded by METROPOLIS *et al.* ([8]). In this calculation, the cascade developed by a pion moving through a Fermi gas of nucleons is followed in a three dimensional geometry. The pion interacts with nucleons according to the observed cross-sections for pions and free nucleons. Energy and momentum are conserved at each interaction. The Pauli principle is taken into account by requiring that the energy of the recoil nucleon be above the Fermi energy for any allowed collision. Pion absorption takes place on two nucleons. For a pion which is not absorbed, the charge, energy, and direction of the pion as it leaves the nucleus are tabulated. A large number of incident pions is followed and the tabulations predict the energy and angular distributions of the inelastically scattered pions, the amount of charge exchange scattering (and double charge exchange, which happens only rarely) and true absorption. Most of the elastic scattering is diffraction scattering or Coulomb scattering and does not appear in the Monte Carlo calculation. Elastically scattered pions which are described by the Monte Carlo calculation appear as transparencies, and emerge from the nucleus undeflected and with unchanged energy. METROPOLIS *et al.* have compared the nucleon cascades with photographic emulsion data with satisfactory agreement indicated ([8]).

In the calculations run for comparison with the present experiment, the nucleonic cascades were ignored. The cross-sections used for the pion-nucleon scattering were $\sigma(\pi^- \mathrm{P}) = (5.3 + 3.5\eta^2 + 3.2\eta^4)$ mb and $\sigma(\pi^- \mathrm{N}) = (3 + 8.75\eta^2 +$

([25]) A. MINGUZZI, G. PUPPI and A. RANZI: *Nuovo Cimento*, **11**, 697 (1954).

$+10.75\eta^4)$ mb, where η is the pion momentum in the laboratory in μc units. The angular distribution of the scattering was taken of the form $a+b\cos\theta+$

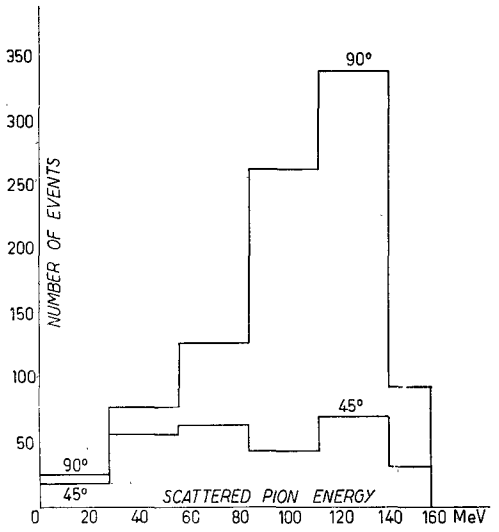

Fig. 7. – Monte Carlo calculation. Energy spectrum of negative pions scattered at 45° and at 90°. The energy of a pion scattered by a free nucleon is 137 MeV at 45° and 102 MeV at 90°.

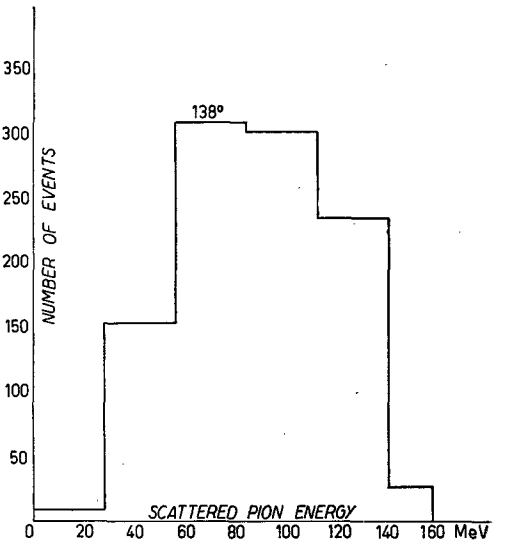

Fig. 8. – Monte Carlo calculation. Energy spectrum of pions scattered at 138°. The energy of a pion scattered by a free nucleon is 77 MeV.

$+c\cos^2\theta$, with the coefficients a, b and c parameterized to give an energy dependence in accord with the available experimental data for each of the types of elementary interaction. The nuclear radius, $r = r_0 A^{\frac{1}{3}}$, was based on $r_0 = 1.569 \cdot 10^{-13}$ cm, and the Fermi energy was taken as 23.8 MeV for both protons and neutrons in carbon. The deaths were estimated by assigning an ab-

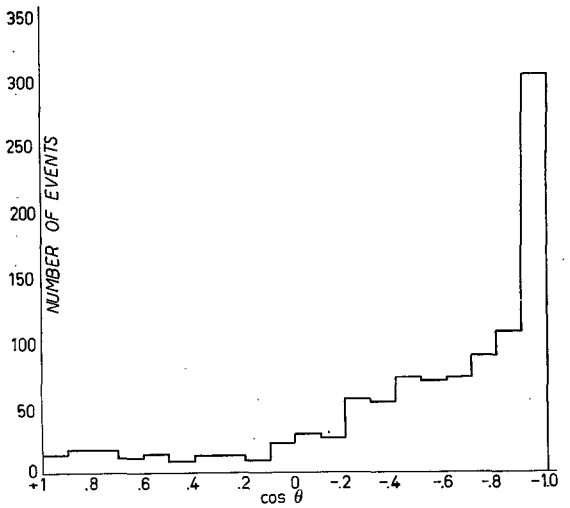

Fig. 9. – Monte Carlo calculation. Angular distribution of scattering in which a 157 MeV incident pion is scattered inelastically with final energy in the range $56 \div 84$ MeV.

sorption cross-section to π^- P collisions according to the arguments of BRUECKNER *et al.* (7). This is expressed in the relation $\sigma_A = \Gamma\sigma_D$, where Γ is a constant determined from experiments at low energy to be about 4, and σ_D is the cross-section for the absorption of pions by the reaction $\pi^- + \mathrm{D} = \mathrm{N} + \mathrm{N}$. The energy dependence of σ_A is assumed to be the same as that of σ_D. The absorption cross-section used was $(18/\eta)(0.14+\eta^2)$ mb (5). The calculations are not completely appropriate for carbon because a Fermi gas description of the nucleons is not accurate and because carbon has a small number of nucleons to treat by this type of statistical method.

The results of the calculations for carbon, which refer to 11390 incident 157 MeV negative pions and to 4200 inelastically scattered negative pions, are summarized in Figs. 7, 8 and 9. The results for lead are the same to within the statistical accuracy to which the calculations were carried.

Figs. 7 and 8 give the energy spectrum in an angular interval which corresponds to the width of the large liquid counter at 45°, 90° and at 138°. The scattering at 45° is depressed because of the Pauli principle. The scattered pions of the Monte Carlo calculation are broadly peaked about the energy of a pion scattered at the same laboratory angle by a free nucleon. The peaking at this energy indicates that most of the scattering proceeded by a single pion-nucleon encounter. The broadening of the peak is a consequence of the Fermi energy of the nucleons in the nucleus. A different momentum distribution would alter the shape of the peak but would not change the energy of the peak very much. The predominance of single encounters is probably a consequence of the Pauli principle (6) and of the smaller pion-nucleon cross-sections at lower energy (1).

The angular distribution of the scattering in the energy interval $56 \div 84$ MeV is shown in Fig. 9. The scattering is preferentially backward. Scattering in this energy interval is typical of that at most energies.

8. – Results.

The energy dependent differential cross-sections, $\mathrm{d}^2\sigma/\mathrm{d}\Omega\,\mathrm{d}E$, for scattering from carbon at several angles are shown in Figs. 10, 11, 12 and 13. Fig. 10, which gives the data at 18.5°, is typical of the scattering from carbon at forward angles as measured with the tapered lucite counter. In Fig. 10, the energies on the half thickness target points are corrected for the difference in ionization losses between the full thickness and half thickness targets. The elastic scattering forms a distinct peak whose width is indicative of the counter resolution. The low sub-peak at 100 MeV shown in Fig. 10 persists through all angles to 45°, but its ratio to the elastic scattering changes by a factor four. Thus, it is unlikely that the lower energy peak is due to some instrumental

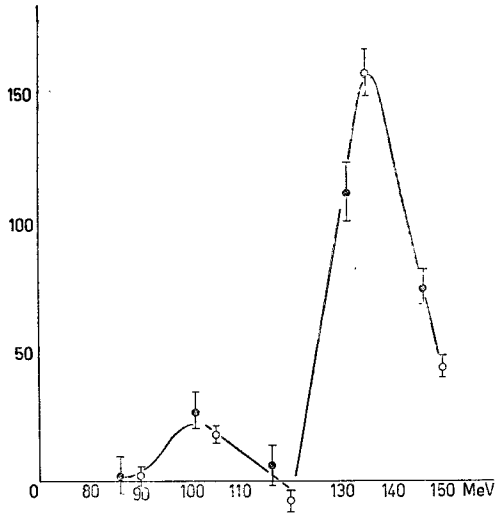

Fig. 10. – Energy analysis of scattering from carbon at 18.5° as measured on the tapered lucite counter. Ordinates in (mb/sr) · 10 MeV. Open circles are full thickness target points; closed circles are half thickness target points. Elastic energy is 138 MeV.

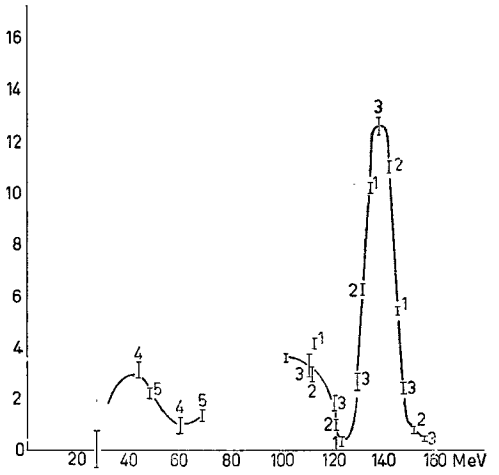

Fig. 11. – Energy analysis of scattering from carbon at 45°, as measured with the liquid Čerenkov and liquid scintillation counters. Points numbered 1, 2 and 3 are different sets of data run with the liquid Čerenkov counter. Points numbered 4 and 5 are the scintillator data analyzed into 6 and 5 energies respectively. The ordinate is (mb/sr) · 10 MeV.

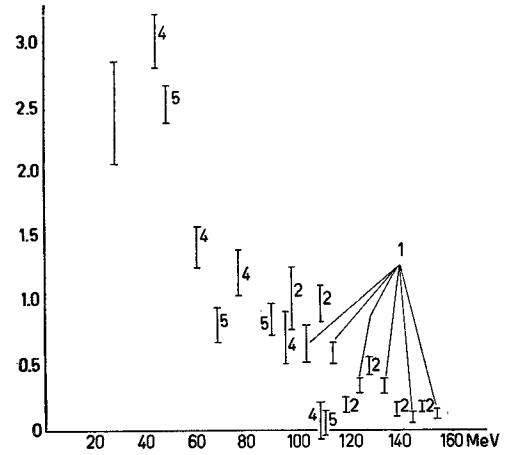

Fig. 12. – Energy analysis of scattering from carbon at 90° as measured with the liquid Čerenkov and liquid scintillation counters. Ordinates and points as in Fig. 11, except points numbered 2 are half thickness target points.

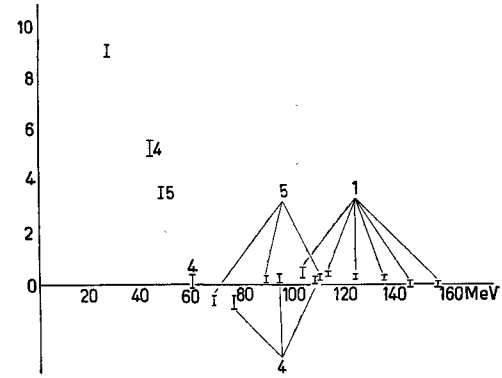

Fig. 13. – Energy analysis of scattering from carbon at 138°. Ordinates and points as in Fig. 12.

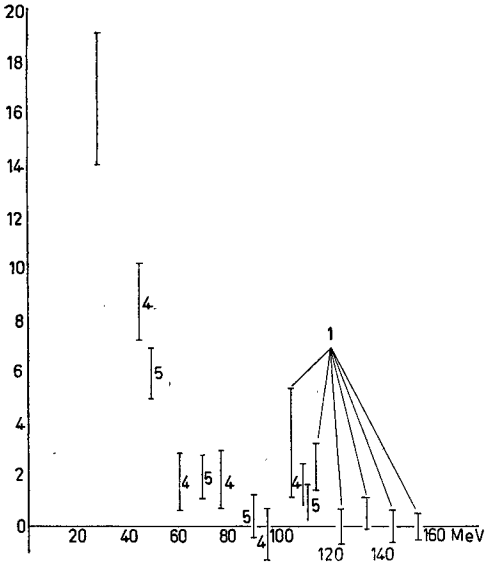

Fig. 14. – Energy analysis of scattering from lead at 90°. Description as in Fig. 11.

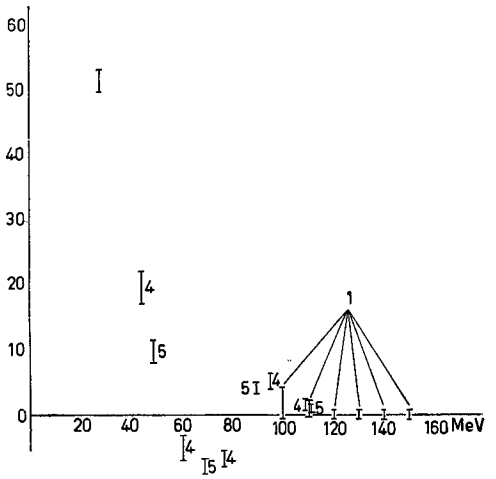

Fig. 15. – Energy analysis of scattering from lead at 138°. Description as in Fig. 11.

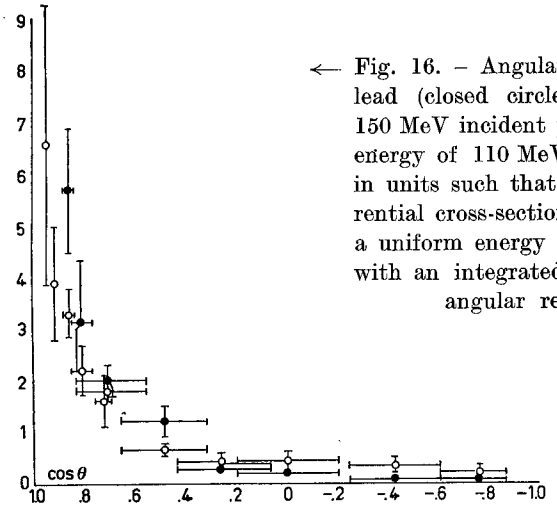

← Fig. 16. – Angular distribution of inelastic scattering from lead (closed circles) and carbon (open circles) in which a 150 MeV incident pion is scattered inelastically with a final energy of 110 MeV. The ordinate, $d^2\sigma/d\Omega\, dE$, is expressed in units such that a value of 1 is the energy dependent differential cross-section of an isotropic angular distribution and a uniform energy distribution from 0 to the full elastic energy with an integrated cross-section equal to the geometric. The angular resolution of the counter is shown.

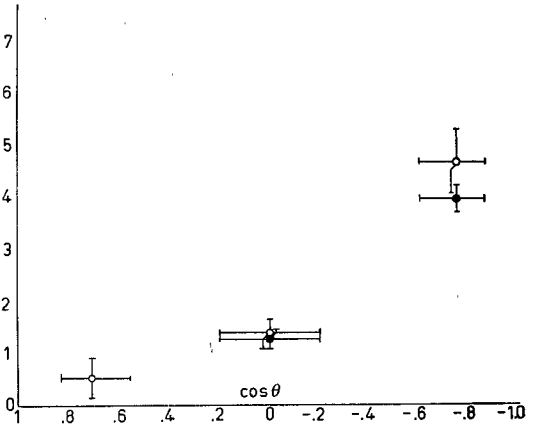

Fig. 17. – Angular distribution of inelastic scattering from lead and carbon in which a 150 MeV incident pion is scattered inelastically with final energy of 30 MeV. Description as in Fig. 16. →

2765

difficulty or a property of the calculation. No multiple scattering effects are noticeable at 18.5° for carbon. Figs. 11, 12 and 13 combine the scintillator data with the liquid Čerenkov counter data to extend the energy analysis down to 30 MeV. The form of the Čerenkov data has the same features as in Fig. 10, but there is a rapid decrease of the elastic scattering with increasing angle, until at 90° and beyond, no elastic scattering is observed above the instrumental background.

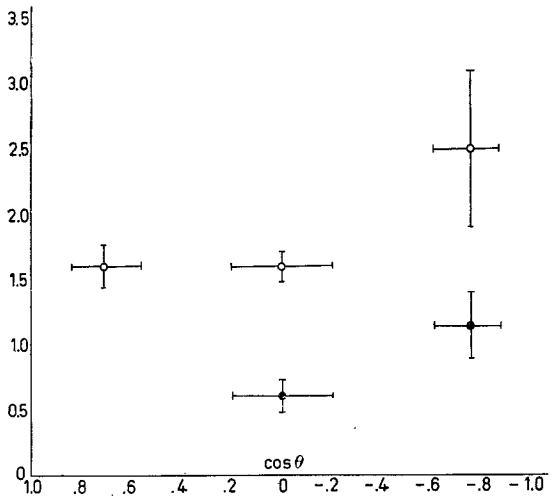

Fig. 18.

The energy dependent differential cross-sections, $d^2\sigma/d\Omega\, dE$, for scattering from lead at 90° and 138° are shown in Figs. 14 and 15. No elastic scattering is observed above the instrumental background.

There is some inelastic scattering in the energy range of the Čerenkov counters at forward angles (Fig. 16) and considerable very low energy scattering in the backwards directions (Figs. 17 and 18). The measured energy spectrum of the pions inelastically scattered from carbon (Figs. 11, 12 and 13) may be compared with the predictions of the Monte Carlo calculations (Figs. 7 and 8), which refer to the same scattering angles. The measured energy of the pions inelastically scattered backwards is about 40 MeV below that predicted by the Monte Carlo calculations. It is interesting to note that the inelastic forward scattering detected by the Čerenkov counters lies about 40 MeV below the energy of a pion scattered from a free nucleon, which is about the same interval by which the backward inelastic scattering is below the pion nucleon scattering at those angles. The general features of the strongly inelastic scattering are the same in carbon and lead, although the inelastic scattering from lead seems to be at a slightly lower energy. This energy difference is probably due to the Coulomb field. Thus it is likely that the inelastic scattering described here is a property of most complex nuclei.

It has been noted in connection with previous experiments ([2,3,26]) that the energy of inelastically scattered pions was considerably below the energy of

([26]) M. Blau and M. Caulton: *Phys. Rev.*, **96**, 150 (1954).

a pion scattered by a free nucleon, which led to the suggestion that the pion may have experienced more than one collision in the nucleus. This experiment indicates that the inelastically scattered pions emerging from nuclei have even lower energy than has been previously reported. However, the Monte Carlo calculations at 150 MeV indicate that events in which the pion suffers more than one collision before leaving the nucleus are improbable. The experimental disagreement with the predictions of the quasi elastic scattering model as

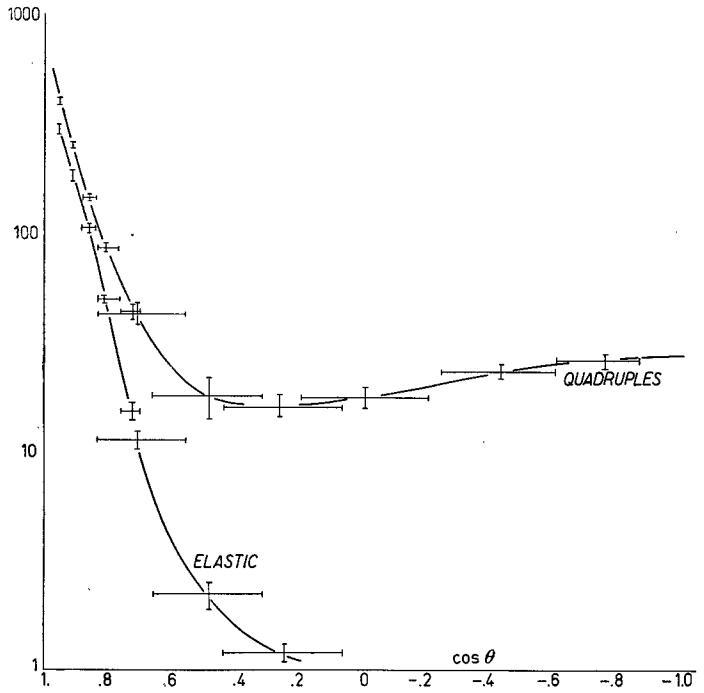

Fig. 19.

worked out in the Monte Carlo calculations is in contrast to the results of the inelastic scattering of protons and electrons ([27,28]) in which the energy of the inelastically scattered particles can be explained by the quasi elastic scattering model. The Monte Carlo calculation does not include many body forces or a potential, either of which may have a significant effect on the scattering. Because of the short mean free path for pions in nuclear matter at this energy, the conditions at the nuclear surface are expected to be important. These may differ from the average conditions within the nucleus which are used in the Monte Carlo calculation.

([27]) J. M. WILCOX and B. J. MOYER: *Phys. Rev.*, **99**, 875 (1955).
([28]) R. HOFSTADTER: *Rev. Mod. Phys.*, **28**, 214 (1956).

The quadruples cross-section includes the scattered pions at all energies above 15 MeV. The angular distribution of the quadruples cross-section (Fig. 19 and 20) shows a slight backward rise, a forward peak due to Coulomb and diffraction scattering, and a broad minimum in the $60° \div 90°$ region. The quadruples differential cross-sections agree favorably with the sum of the elastic and inelastic differential cross-sections as given by KESSLER and LEDERMAN ([3]) at 125 MeV, but are almost double the values given by the Russian

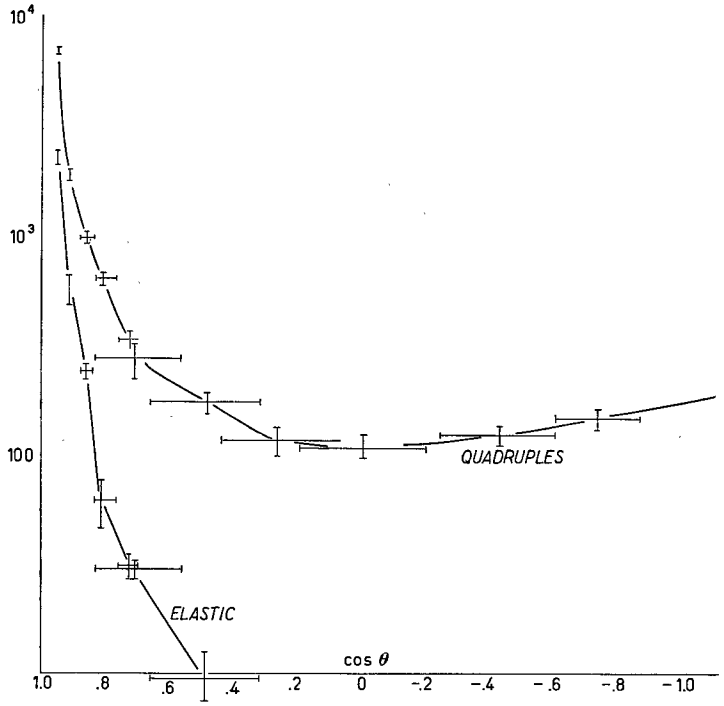

Fig. 20.

cloud chamber group ([2]). The comparison with the Russian data thus indicates that the total scattering cross-section decreases by about a factor two between 150 and 240 MeV, in rough agreement with the cross-sections for pion-nucleon scattering. This feature is in rough agreement with the trends of transmission experiments at higher energies ([2]), and lends support to the quasi elastic scattering model.

The total cross-sections determined in this experiment are tabulated in Table V. The geometric cross-sections given use $\sigma_{ge} = \pi r_0^2 A^{\frac{2}{3}}$, with r_0 equal to a pion Compton wave length, and include the Coulomb correction for negative pions ([29]). The errors listed are standard deviations.

([29]) R. M. STERNHEIMER: *Phys. Rev.*, **101**, 384 (1956).

The quadruples cross-section given in Table V is the quadruples differential cross-section integrated over the solid angle outside the transmission counter. The difference between the attenuation and quadruples cross-sections represents absorption and charge exchange events to which the counters are not sensitive.

TABLE V. – *Total cross-sections (millibarns).*

Cross-sections	Target	
	Carbon	Lead
Geometric	329	2425
Attenuation	542 ± 28	2750 ± 150
Quadruples	350 ± 20	2370 ± 150
Absorption + Charge exchange . .	192 ± 34	380 ± 310
Charge exchange [3]	20	100
Absorption	172 ± 35	280 ± 310
Absorption/geometric	0.52 ± 0.11	0.12 ± 0.13
Monte Carlo, deaths/events . . .	0.42	0.54
Elastic	110 ± 30	263 ± 27
Inelastic processes	430 ± 42	2490 ± 160

The two effects cannot be separated in this experiments so the charge exchange cross-sections of KESSLER and LEDERMAN [3] have been subtracted to give the absorption cross-sections of Table V. The ratio of absorption to geometric cross-section is given for comparison with the ratio of deaths to total events from the Monte Carlo calculations on carbon and lead. The absorption in carbon is in fair agreement with the Monte Carlo, but in lead the Monte Carlo predicts four times the observed absorption. The absorption cross-section deduced for lead is small because the cross-section determined from the quadruples count is large. It is possible that the corrections for protons and γ-rays as estimated in Sect. 6 are satisfactory for carbon but inadequate for lead. It is a weakness in the experimental method that it does not allow for the independent determination of these corrections, which accordingly must be verified by comparison of the present results with the results of other experiments. The previously mentioned agreement with the sum of the elastic and inelastic differential cross-sections of KESSLER and LEDERMAN [3] for 125 MeV π^- on lead was taken as corroboration of the quadruples cross-section determined in this experiment. The small absorption deduced for lead relative to that predicted by the Monte Carlo calculation implies that the absorption probability assigned to a collision of a negative pion with a nuclear proton, without regard for factors such as nuclear size, is not an adequate description of the actual absorption process [30].

[30] The values of the ratio $g=(\sigma_{ab})/(Z\sigma_D)$ obtained in this experiment are 2.5 ± 0.5 for carbon and 0.29 ± 0.32 for lead. The corresponding values from the Monte Carlo

The elastic cross-section given in Table V is the elastic differential cross-section integrated over the solid angle outside the transmission counter. The elastic cross-section is smaller than has been previously reported ([2,3]) probably because of the more stringent definition of elastic scattering used in this experiment. The difference between the attenuation and elastic cross-sections is the cross-section for inelastic processes, which is somewhat uncertain because of the forward inelastic scattering. The cross-section for inelastic processes in carbon is greater than geometric by $2\frac{1}{2}$ standard deviations. The cross-section for lead is essentially geometric. The observed cross-section for inelastic processes is larger than that calculated from the optical model with reasonable values of the real and imaginary parts of the optical potential ([5]) by a partial waves solution including the Coulomb field and using a square well whose radius is based on the pion Compton wave length ([9]). The application of the experimental results regarding the angular distribution of the elastic scattering and the measured large value of the cross-section for inelastic processes to the determination of optical model parameters is discussed by FUJII ([9]).

9. – Conclusions.

The inelastic scattering of negative pions is preponderantly backward and is characterized by great energy losses. The energy of inelastically scattered pions leaving a nucleus is considerably lower than predicted by the quasi elastic scattering model in a Monte Carlo calculation based on a simple Fermi gas model. This is in contrast to the experimental results regarding the scattering of protons and electrons, in which the quasi elastic scattering model gives correctly the energy of the inelastically scattered particles. Furthermore, the absorption of pions in lead is less than that predicted by the Monte Carlo calculation by a factor of four.

* * *

It is a pleasure to acknowledge the advice and assistance of Professor H. L. ANDERSON, who suggested this problem. Professors S. C. WRIGHT and

---

calculation are 1.94 and 1.18. These values combine with the corresponding values of. LEDERMAN *et al.* (ref. ([3])) for carbon at 62 MeV, $\Gamma \gtrsim 3.3$; and of TENNEY and TINLOT (*Phys. Rev.*, **92**, 974 (1953)) for beryllium, $\Gamma = 3.2^{+1.1}_{-0.8}$ at 39 MeV and $\Gamma = 5.6^{+2.1}_{-1.1}$ at 20 MeV to form a straight line through the origin when plotted against $1/kR$. The slope of this line, including values of g derived from the absorption cross-sections quoted by TRACY (*Phys. Rev.*, **91**, 960 (1953)) and by SAPHIR (*Phys. Rev.*, **104**, 535 (1956)) is $g=(7.4\pm0.6)/kR$ at a 20% level of confidence by a least squares fit. The pion wave number is k, and R is the nuclear radius.

A. TURKEVICH of the University of Chicago and Dr. W. C. DAVIDON of the Argonne National Laboratory assisted with many helpful discussions. The writer is grateful to Dr. DONALD FLANDERS and JEAN HALL of the Argonne National Laboratory for making the AVIDAC available for computing energy analyses. Drs. N. METROPOLIS, M. STORM and R. BIVINS of the Los Alamos Scientific Laboratory very kindly conducted the MANIAC calculations of several thousand events by the Monte Carlo method for carbon and lead targets. Mr. T. FUJII assisted in assembling the equipment, conducting the experiment, and the subsequent analysis of the data. Mr. J. FAINBERG was very helpful during the runs. The efforts of Mr. C. BORDEAUX and the cyclotron operating staff through several weeks of around-the-clock runs are gratefully acknowledged.

RIASSUNTO (*)

Si sono usati contatori di Čerenkov o a scintillazione sensibili all'energia collegati ad un analizzatore dell'altezza degli impulsi per misurare lo spettro d'energia di pioni negativi di 150 MeV dopo scattering a vari angoli su carbonio o piombo. La maggioranza dei pioni si trovò nell'emisfero posteriore con energia inferiore a 40 MeV. Ciò è in contrasto coi risultati di un Montecarlo basato su un semplice modello di un gas di Fermi in cui la maggioranza dei pioni diffusi all'indietro hanno energie superiori a 60 MeV. Le misure indicano che l'assorbimento dei pioni in carbonio corrisponde approssimativamente a quello predetto dal Montecarlo, mentre l'assorbimento in piombo è circa $\frac{1}{4}$ del previsto.

(*) *Traduzione a cura della Redazione.*